Transparent and flexible ECoG electrode arrays based on silver nanowire networks for neural recordings

Joana P. Neto[1,2,*], Adriana Costa[1], Joana Vaz Pinto[1], André Marques–Smith[2], Júlio Costa[1], Rodrigo Martins[1], Elvira Fortunato[1], Adam Kampff[2,*] and Pedro Barquinha[1,*]

[*] joanasneto@gmail.com, adam.kampff@gmail.com, pmcb@fct.unl.pt

[1] CENIMAT/I3N and CEMOP/Uninova, Departamento de Ciência dos Materias, Faculdade de Ciências Tecnologia–Universidade Nova de Lisboa, Caparica, Portugal

[2] Sainsbury Welcome Centre for Neural Circuits and Behaviour, University College London, United Kingdom

Abstract

This work explored hybrid films of silver nanowires (AgNWs) with indium-doped zinc oxide (IZO) for developing high-performance and low-cost electrocorticography (ECoG) electrodes.

The hybrid films achieved a sheet resistance of 6 Ω/sq while maintaining a transparency of ≈60% at 550 nm. Electrodes with 500 µm diameter were fabricated with these films and reached an impedance of 20 kΩ at 1 kHz and a charge storage capacity of 3.2 mC/cm^2, a 2× and 320× improvement over IZO electrodes, respectively. Characterization of light-induced artifacts was performed showing that small light intensities (<14 mW/mm^2) elicit electrical potential variation in the magnitude order of baseline noise. The validation of electrodes in vivo was achieved by recording electrical neural activity from the surface of rat cortex under anaesthesia. Moreover, the presence of the films did not cause obstruction of light during fluorescence microscopy.

The presented film and electrode characterization studies highlighted the capabilities of this hybrid structure to fabricate transparent and flexible electrodes that are able to combine the superior temporal resolution of extracellular electrophysiology with the spatial resolution offered by optical imaging.

Introduction

Understanding how distributed populations of neurons coordinate their activity to generate behavior in animals will require tools capable of simultaneously monitoring neural activity on a large, precise and fast scale across multiple brain areas, ideally with the added ability to resolve genetically-distinct types of neuron (Buzsáki, 2004; Yuste, 2015). In the past decades, technological advances have provided neuroscientist powerful tools for simultaneously monitoring the activity of hundreds to thousands of neurons in vivo.

One such tool is functional calcium imaging (wide-field and two-photon imaging). The activity of genetically-identified neurons can be detected optically using fluorescent calcium-sensitive dyes or proteins into the cell membranes of neurons. The primary strength of imaging approaches is their spatial resolution, allowing the relative locations, and the cell-type or connectivity of the neurons, to be obtained. The drawback of imaging-based approaches for recording neural activity is their poor temporal resolution (rise times of ~10-50 ms for single action potentials) (Harris, Quiroga, Freeman, & Smith, 2016; Scanziani & Häusser, 2009).

How can we monitor large-scale neuronal activity dynamics with high spatio-temporal resolution?

Extracellular recording (electrical recording) remains the only technique capable of measuring the activity of many neurons simultaneously with sub-millisecond precision (Dimitriadis et al., 2018). Flexible electrode arrays (EAs) can cover the cortical surface providing a view of large-scale activity of distributed populations of neurons with high temporal resolution and minimal brain damage. However, the recorded signal cannot reveal exact locations of active neurons, and can only provide cell-type information if used in combination with photostimulation (Lima, Hromádka, Znamenskiy, & Zador, 2009), which is laborious and low-throughput. Each electrode is sensitive to the activity of hundreds of neurons in its vicinity (Neto et al., 2016).

Simultaneous recordings of neural electrical activity on a large and fast scale with direct visualization of neurons could provide insight into how the brain works and to better understand the nature of the electrophysiological recorded signal and have an impact on clinical and brain-machine research where ECoG is frequently used.

There have been promising attempts to build transparent ECoG electrodes using tin doped indium oxide (ITO) and graphene. An array with 49 ITO electrodes (500 µm diameter) was tested in vivo (P Ledochowitsch et al., 2015). Thunemann et al. have recently reported the use of graphene in ECoG electrodes (Thunemann et al., 2018). Arrays with 16 graphene electrodes (100×100 µm separated by 300 µm) enabled simultaneous 2-photon microscopy, optogenetic stimulation, and cortical recordings.

While graphene presents remarkable properties, its fabrication by reproducible and large-scale methods is still challenging. Regarding ITO, due to indium scarcity and brittleness a number of lower cost alternatives are currently being study for solar cells and displays. These include, conductive polymers, carbon nanotubes and metallic nanostructures - metal nanowires, thin metal films and patterned metal grids (Hecht, Hu, & Irvin, 2011). Recently, transparent ECoG electrodes have been fabricated with patterned metal grids demonstrating high-performance and hence showing that metal nanostructures are a promising material for transparent electrodes on flexible substrates (Qiang et al., 2017; Seo et al., 2017). In our work we have fabricated transparent electrodes with Silver Nanowires (AgNWs) and IZO, which enables a transparent and conductive hybrid structure. Metal nanowires networks maintain the advantages of patterned metal films adding simpler and lower cost manufacturing available with solution-based deposited techniques. Moreover, IZO coating works as corrosion inhibitor to prevent the slow degradation of the silver nanowire film conductivity over time, whilst also

improving nanowire adhesion to substrate and electrical connectivity of the network (Lee et al., 2013; Yun et al., 2016).

Therefore, the motivation for this work comes from the need to explore emerging materials to advance transparent ECoG electrodes enabling new combinations of electrophysiology and imaging.

Methods

Fabrication and characterization of transparent and conductive films

Glass and silicon wafers were sonicated sequentially in acetone and isopropyl alcohol (IPA) for 15 minutes, rinsed with ultra-pure water, and finally dried with a stream of N_2.

IZO films (In_2O_3/ZnO, 89.3/10.7 wt%, 3'' ceramic targets from SCM, Inc.), of 100 and 200 nm, were deposited in a homemade RF magnetron sputtering system at RT. The Oxygen partial pressure and the deposition pressure ($Ar + O_2$) were kept constant at 1.5×10^{-3} Pa and 1.0×10^{-5} Pa, respectively. The target–substrate distance and RF power were kept constant at 15 cm and 50 W, respectively. To obtain films of 100 and 200 nm the deposition time was set to 40 minutes and to 80 minutes, respectively. Additionally, a second protocol was used to fabricate 200 nm films, to avoid the risk of damaging the substrate, Parylene C. Therefore, the deposition was made in steps: 40 minutes sputtering on, 25 minutes sputtering off and 40 minutes sputtering on.

Commercial AgNWs (115 nm diameter and 20-50 µm length) purchased from Sigma Aldrich were used with a concentration of 1.44 M. AgNWs were spray coated at 1 ml/min, directed by a stream of dry Nitrogen gas at 7 Bar, onto clean glass substrates on a heated stage (150 ± 10 °C) using an ultrasonic spray head (Sonotek, 0.8 W), with raster pattern designed to maximize uniformity over the sample area (see in supplementary information Figure 1 the pattern of one cycle of spray deposition). The control of network density was achieved by using a homemade in situ resistance monitor made using 2.5 ×2.5 cm^2 glass substrate, copper tape connected at the Ohmmeter and Silver paste to connect from copper to the glass substrate.

The optical, electrical and morphological properties of the films were analyzed. The optical transmittance measurements were taken with a PerkinElmer Lambda 950 UV/VIS/NIR Spectrometer. The measurements were performed using an integrating sphere (measure the total transmitted light) in the wavelength range from 200 nm to 1500 nm. Samples with a Van der Pauw structure were used in a Hall Effect System (BioRad HL5500) with a 0.5 T permanent magnet to access their sheet resistance at room temperature. The thickness of IZO was measured by profilometry using an Ambios XP-200 profilometer. The surface morphology was investigated using Scanning Electron Microscopy (SEM, Zeiss Auriga Crossbeam microscope) and Atomic force microscopy (AFM) analysis was performed using an Asylum Research MFP-3D Stand Alone AFM system. SEM images were also used to calculate the areal mass density (amd) and the calculation assumes that the NWs network was homogenous. Topography measurements were performed in tapping (alternate contact) mode in air, using commercially available silicon AFM probes (Olympus AC160TS; k = 26 N/m; f_0 = 300 kHz).

Production and characterization of electrode arrays

Following films characterization implantable neural electrode arrays were fabricated. Firstly, Silicon carrier wafers were coated with PVA to help the peel-off process latter. The solution of PVA (100 mL of H_2O with 5 g of PVA 88% hydrolyzed, average M.W. 20,000-30,000) was prepared on a hot plate at 80° C, where PVA was slowly added to the water at 80° C and stirred

at 500 rpm for a few hours. Then, PVA was spin-coated for 60 s at 1000 rpm with acceleration of 200 rpm/s. At the end, the silicon wafer was moved to a hot plate at 95° C for 5 minutes. In the second step of the process, a ~5 µm thin layer of Parylene C (poly(para-chloro-xylylene) (8.5 g) was deposited using a Specialty Coating System Model 2010. In the third step, for the hybrid electrodes AgNWs were deposited onto the Parylene substrate and patterned using shadow masking to form electrodes, connection pads and interconnect lines. These masks were fabricated from a 1 mm thick aluminum sheet, where the pattern was cut by a Gravograph IS400 with the blade positioned at a 10˚ angle to the perpendicular surface. The AgNWs network was then coated with a 100 nm thick IZO film to protect against oxidation/degradation. The connection pads area was protected during IZO deposition. For the IZO-only electrodes a film of 100 or 200 nm was deposited and patterned using shadow masking. In the fourth step, the connection pads to zero insertion force (ZIF)connectors and initial portions of the interconnect lines (excluding the electrode area) were prepared with Ti (± 6 nm) and Au (± 60 nm) via Electron Beam Evaporation using shadow masking. Au was used to reduce line resistance and to improve the contacts between the devices and the ZIF connectors, whilst Ti was used to improve Au adhesion. Next, a ~1 µm thick passivation/insulating layer of parylene C (2 g) was deposited. Plasma etching (RIE Trion Phantom III) was then used for etching Parylene C passivation layer, simultaneously opening windows for the electrodes and contact/ZIF interfaces. Finally, the arrays were released from the silicon carrier wafer by scratching the borders of the carrier and immersing in de-ionized water at 90° C for around 1 h (PVA started to dissolve and Parylene C to detach from the silicon wafer). Kapton tape was added to the back of the pad region of each device to increase the thickness ensuring a good electrical connection to the ZIF connectors on the PCB.

The electrochemical behavior of the microelectrodes was studied in PBS (1 mM, pH 7.4) by Electrochemical Impedance Spectroscopy (EIS) and cyclic voltammetry. Electrodes were immersed in PBS and a NanoZ (Neuralynx) was used to characterize impedance, with a two electrode cell configuration - electrodes acted as working electrode and an Ag/AgCl wire as reference electrode (Science Products GmbH, E-255). Moreover, the impedance magnitude at 1 kHz of each electrode was also measured using a protocol implemented by the RHD2000 series chip (InTan Technologies). For the cyclic voltammetry, a potentiostat (Reference 600, Gamry Instruments) was used with a three electrode cell configuration where the electrodes were connected individually as the working electrode, a platinum wire served as the counter electrode, and an Ag-AgCl (3 M KCl, Gamry Instruments) as the reference electrode.

We measured the light-induced artifacts by immersing electrodes into PBS solution while using an Ag-AgCl wire as a reference (Science Products GmbH, E-255). We then used a fiber-coupled Light Emission Diode (LED) (LED 470 nm, fiber cable-SMA to 1.25 mm ferrule, and fiber optic cannula- 200 µm, 0.39 NA, Thorlabs) to deliver blue light. By touching with the fiber tip on the microelectrode surface, artifacts were quantified from noise recording in the form of potential peaks. We studied the dependence of the amplitude of artifacts on different light intensity using a 10 ms pulse duration at 1 Hz. A power meter measured the light intensity used, which ranged from 14 to 95 mW/mm^2. To drive the LED intensity and pulses a Pulse Pal (Sanders & Kepecs, 2014) and Bonsai workflow (Lopes et al., 2015) were used to enable precise sequences of voltage pulses. For the signal recordings we used the Open Ephys (http://www.open-ephys.org) acquisition board along with the RHD2000 series interface chip that amplifies and digitally multiplexes the signal from the 32 extracellular electrodes (Intan Technologies). Extracellular signals in a frequency band of 0.1-7,500 Hz were sampled at 20 or 30 kHz with 16-bit resolution and were saved in a raw binary format for subsequent offline analysis using Bonsai interface.

Characterization of electrodes in vivo – neural electrical recordings

The protocol was followed as described in previous works for urethane acute recording surgeries on rats (Neto et al., 2018). A craniotomy was made over the left hemisphere, ~1-7 mm posterior and ~1 to 4 mm lateral to bregma. The transparent electrodes were positioned around 3 – 5 mm posterior relative to bregma, which in cortex covers motor cortex (M), primary somatosensory cortex (S1), parietal cortex (PtA), and secondary visual cortex (V2).

Optical Imaging characterization

Biological specimens for imaging were obtained from a C57Bl6 mouse (Charles River Labs, UK) expressing mCherry sparsely in neurons of the Lateral Posterior nucleus of the thalamus (LP) and several areas of the neocortex.

The mouse had previously been transcardially perfused under terminal general anaesthesia with 0.1M phosphate-buffered saline (PBS), followed by 4% paraformaldehyde (PFA) in PBS and the brain dissected from the cadaver. After 24h post-fixation in 4% PFA, the brain had been embedded in 4% agarose and 40 µm-thick brain slices were cut using a vibratome. To visualise cell nuclei, slices were incubated in Hoechst solution (20 mM, ThermoFisher Scientific UK, 33342) for 15 minutes and then washed 4 times in 0.1M PBS. Slices were mounted on glass slides, air-dried, covered in ProLong Glass Antifade Mountant (ThermoFisher Scientific UK, P36980) and then cover-slipped. The cover-slips were coated with the films under study.

Imaging was performed in a Zeiss AxioImager 2 microscope (Apotome optical sectioning mode, 0.61 µm optical sections) under a Plan-Neofluar 20x/0.5 NA objective (Carl Zeiss, Jena, Germany).

Analysis

Python software was used to calculate the average peak-to-peak (P2P) amplitude of the light induced artifacts on a given electrode, where the Pulse Pal analog signal was used for synchronization. Additionally, signal processing was used, such as filtering and calculation of noise in saline solution as the standard deviation (root-mean-square noise) of the signal. Some results were represented as mean ± standard deviation.

Results

Transparent ECoG electrodes should have high transparency and low impedance (Kozai & Vazquez, 2015) being able to sense cortical local field potentials (LFPs).

Characterization of transparent and conductive films

Figure 1 A and B illustrate transmittance spectrum in the wavelength range from 250 to 1200 nm for IZO and hybrid films (AgNWs with IZO), respectively. Being transparent for optical imaging is important because it means that a large percentage of light is transmitted through the film in both directions enabling excitation and emission light.

The thickness measured of IZO films was around 100 nm (142 ± 17 nm, n= 4) and 200 nm (224.8 ± 52 nm, n=4). If we target for transmittance at 550 nm (standard value), the IZO 100 and 200 nm films presented a value of 81.8 ± 0.5 % and 75.5 ± 1.1 %, respectively. For the hybrid films, the transmittance at 550 nm decreased as more AgNWs are deposited. The AgNWs films with 11 and 20 cycles showed transmittances of 84.3 % and 76 % at 550 nm, respectively. The transmittance in the hybrid structure with AgNWs 11 cycles was 73.8 % and

61.7 % for the hybrid structure with AgNWs 20 cycles. In general, AgNWs films showed higher transmittance than hybrid films. Overall, AgNWs, IZO and hybrid films showed transmittances at 550 nm over 60 %, which is acceptable for optical imaging (Lu et al., 2018). Moreover, all the films demonstrated moderate-to-high transmittance all throughout the 400-1100 nm optical window with a transmittance above 60 %. High transmittance in this broad frequency range enables different imaging techniques, such as widefield microscopy (~400-600 nm), two-photon microscopy (~800-1100 nm), and optogenetics (~470 nm) applications (Seo et al., 2017).

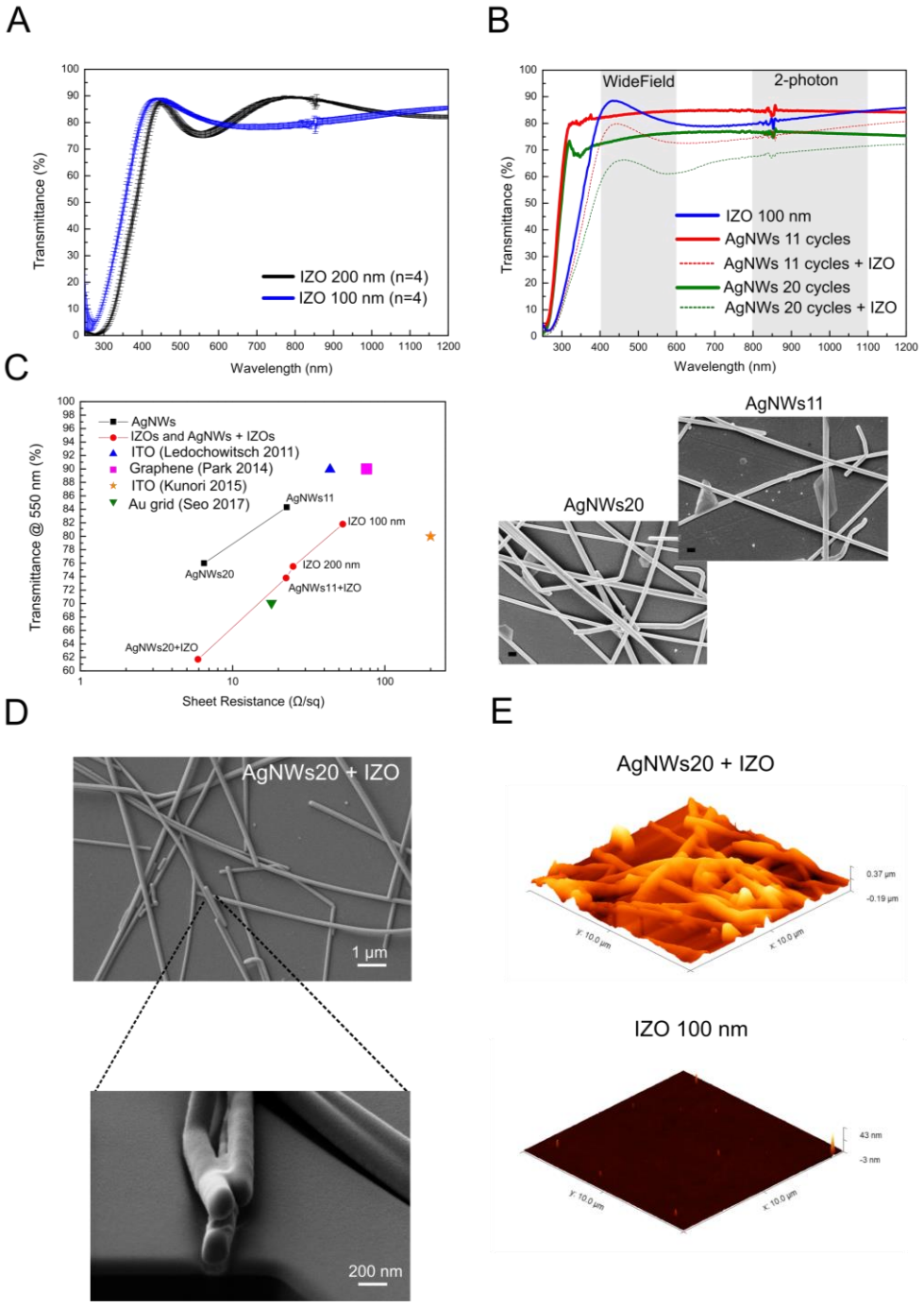

Figure 1. Film characterization. (a) Optical transmittance of IZO films with thickness of 100 and 200 nm. Four films were fabricated for each condition; (b) Optical transmittance of AgNWs and hybrid films. The wavelength range used in widefield and two-photon microscopy is shown in grey shadow; (c) Transmittance at 550 nm versus sheet resistance for various conducting materials (IZO, AgNWs, hybrid AgNWs + IZO, and films from literature). Inset:

SEM images of AgNWs 11 cycles and AgNWs 20 cycles films (scale bar = 200 nm); (d) SEM image of AgNWs 20 cycles with IZO 100 nm film. Bottom image shows a cross section of the film; (e) AFM images of AgNWs 20 cycles with IZO 100 nm and IZO 100 nm films.

The electrical properties of IZO, AgNWs and hybrid films were measured by Hall Effect. Figure 1 C summarizes transmittance values at 550 nm as a function of sheet resistance from these films along with values reported in the literature for ITO (Ledochowitsch et al. 2011; Kunori and Takashima 2015), Graphene (Park et al., 2014) and patterned metal grids (Seo et al., 2017). As expected, a tradeoff exists between conductivity and transparency. By increasing the thickness/density of material, the conductivity is increased but the transparency is decreased.

The sheet resistance and the transparency values achieved by our hybrid structure - AgNWs11 + IZO- were similar to the metal grids (Seo et al., 2017). Generally, our films when compared with other works, presented a lower sheet resistance but also a lower transmittance. For instance, for a given sheet resistance of ~40 kΩ/sq, ITO films (Ledochowitsch et al. 2011) showed 90% transmittance while IZO films showed 80% transmittance. This comparison indicates that the light transmittance is slightly less in our films when compared with the most used TCO for a given sheet resistance. Nonetheless, a key vision for ECoG electrodes is large-scale and high-density. A critical aspect when fabricating these arrays are the interconnects that will become long yet narrow. The hybrid films have demonstrated much higher conductivity than the other films. Moreover, from the plot in Figure 1 C we may conclude that the sheet resistance in hybrid structures is controlled by the sheet resistance of the AgNWs films. In the AgNWs films the sheet resistance varies with the number of AgNWs deposition cycles and consequently with the areal mass density (amd). Inset images in Figure 1 C show SEM images and how the density of nanowire network is achieved through the number of deposition cycles, where calculated amd values for 11 and 20 deposition cycles were 82 and 149 mg/m^2, respectively. For 11 and 20 cycles of deposition, the density is above the percolation threshold of the network (percolation threshold is around 50 mg/m^2). As is evident from the insert images in Figure 1 C, the AgNWs are randomly oriented and interconnected enabling high conductance.

As shown in Figure 1 D, the morphology of hybrid films, which are composed by AgNWs and IZO 100 nm coating, appeared identical to the uncoated ones, suggesting the IZO coating is covering perfectly the AgNWs network. The diameter of AgNWs before coating is around ~128 nm and after is ~190 nm. The IZO coating helps to reinforce the connectivity between the nanowires network (inset in Figure 1 D) and improve their adhesion to the substrate. Nevertheless, the conductivity in the hybrid structure is mainly ensured by the AgNWs network as can be observed in Figure 1 C.

The morphology of the coated nanowires was additionally analyzed through AFM (Figure 1 E). AFM images are in good agreement with the SEM results. Figure 1 E showed how the roughness of the surface and the superficial area increases in the hybrid structure when comparing with the IZO 100 nm film.

Characterization of transparent and conductive electrodes

Figure 2 A and B illustrate a schematic of the electrodes array and a schematic of the fabrication layers with a hybrid film, with Parylene C as substrate (thickness, 5 µm) and encapsulation (thickness, 1.5 µm) layer, with Ti/Au as the contact pads and initial portions of the interconnect lines (thickness, 6/60 nm), and with IZO (thickness, 100 nm) and AgNWs (11 or 20 cycles) as the electrodes and interconnects lines. The final device is flexible due to its final thickness, less than ~ 7 µm (Figure 2 C).

.

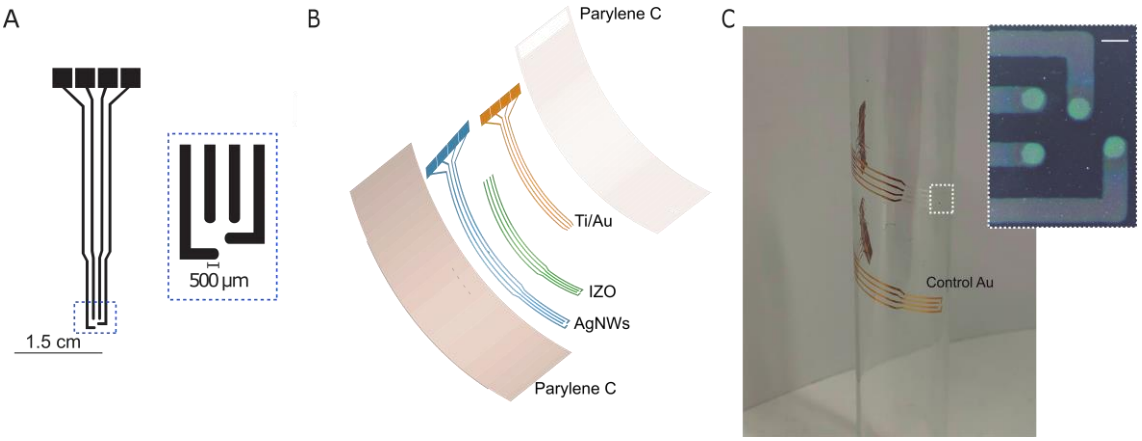

Figure 2. Electrode fabrication and overview. (a) Design of electrode arrays. The inset shows a magnified view of the array, consisting of 2 x 2 electrodes (diameter 500 µm); (b) Diagram of electrodes construction showing the flexible layered structure; (c) Demonstration of device flexibility. Devices are wrapped around a glass tub with a diameter of 2.5 cm. A gold (Ti/Au) device was also tested as control. Inset: close-up of 4 electrodes. Scale bar: 500 µm.

Figure 3 shows the detailed electrochemical characterization of the electrodes. The impedance at 1 kHz is a common metric for assessing the performance of microelectrodes (Figure 3 A). The impedance of IZO 100 nm, IZO 200 nm, AgNWs11 + IZO, AgNWs20 + IZO at 1 kHz was 452 ± 200 kΩ, 41 ± 65 kΩ, 23 ± 5 kΩ, and 20 ± 2 kΩ, respectively. The impedance values at 1 kHz for the electrodes produced with the IZO 200 nm and hybrid structure presented the lower values. Nevertheless, the difference between the hybrid structure with 11 cycles and 20 cycles is very small, ~ 10%. For further analysis, the cyclic voltammetry (CV) results of IZO 200 nm and hybrid structures appear in Figure 3 B. The enclosed area of CV curves defines the charge storage capacity (CSC) of the electrodes. From Figure 3 B, it is clear that the CSC value increases significantly with AgNWs density in the hybrid structure. The CSC derived from curves in Figure 3 B is 0.01 mC/cm^2 for IZO 200 nm electrodes, 0.5 mC/cm^2 for AgNWs11 + IZO electrodes and 3.2 mC/cm^2 for AgNWs20 + IZO electrodes. The CSC value for AgNWs20 + IZO electrodes is much higher when compared with the CSC value for the metal grids electrodes (CSC < 1.41 mC/cm^2)(Qiang et al., 2017). The increase in the superficial area, due to the increase in the AgNWs density, may explain the difference of CSC values between electrodes. Increased CSC for hybrid structures could enhance the amount of transferred charge when electrodes are used for neural stimulation. Furthermore, judging from the electrochemical impedance spectroscopy (EIS) measurements performed on electrodes, in the plot of phase as a function of frequency, as shown in Figure 3 supplementary information, the impedance became more capacitive (phase closer to 90°) due to the presence of AgNWs in the film. The overall impedance decreased as the electrode surface became rougher, probably due to the increased effective electrode surface area with enhanced charge transfer (Chung et al., 2015).

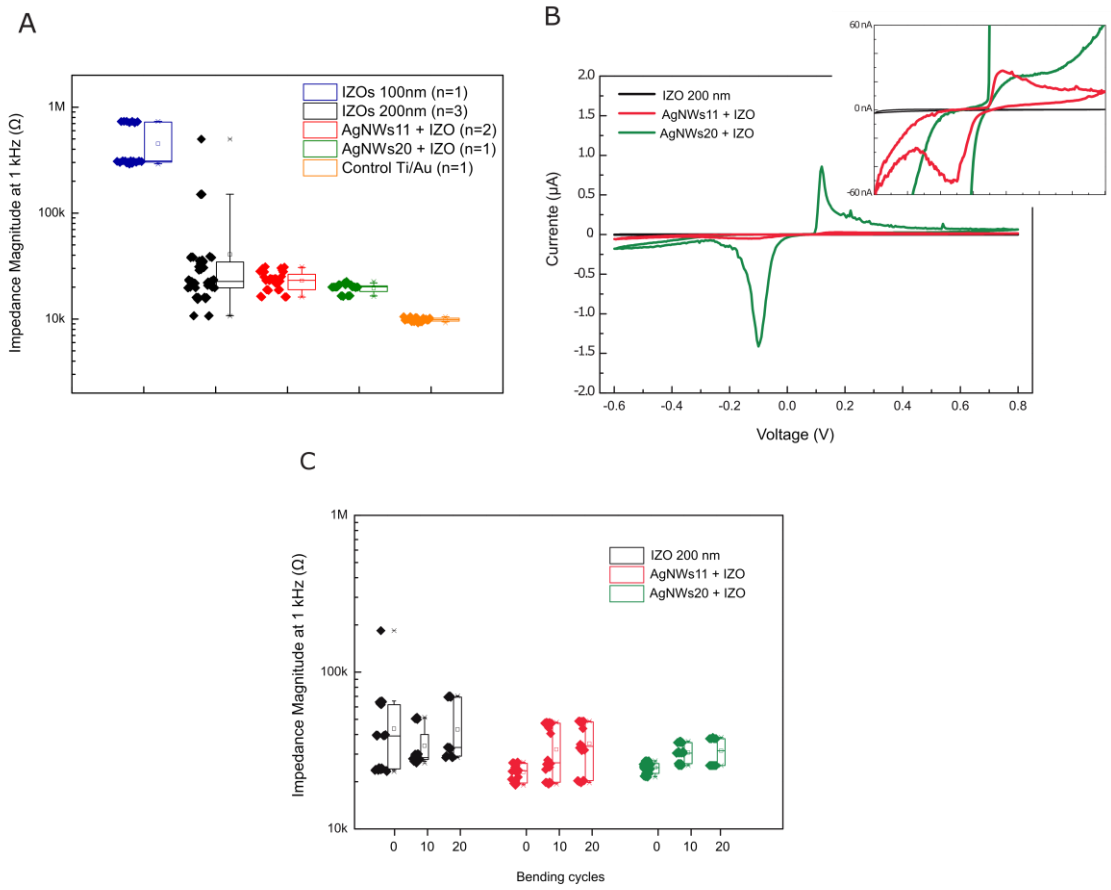

Figure 3. Electrodes electrochemical characterization. (a) Impedance magnitude measured at 1 kHz in saline as a function of different electrodes and prototypes (n denotes the number of prototypes); (b) Cyclic voltammetry (3rd curve) (c) Impedance magnitude measured at 1 kHz in saline as a function of a bending cycles with a bending diameter of 2.5 cm. Points denote impedance magnitude measured at 1 kHz in saline solution for individual electrodes, and boxplots show the distribution of these values. In the boxplots, line: median, square: mean, box: 1st quartile–3rd quartile, and whiskers: 1.5× interquartile range above and below the box.

Mechanical flexibility of a transparent microelectrode is also of great importance. In this work, we performed bending tests with both IZO 200 nm and AgNWs + IZO microelectrodes. Figure 3 C demonstrates the impedance change after up to 20 bending cycles. There was only slight change of impedance after 20 bending cycles, indicating the flexibility of our devices. Electrodes impedance with IZO 200 nm changed from 44 to 43 kΩ (yield 73%), with AgNWs11 + IZO from 23 to 35 kΩ (yield 100 %), and with AgNWs20 + IZO from 25 to 29 kΩ (yield 67 %). It should be possible to improve the yield value improving the mechanical stability by changing the thickness of the substrate and passivation layer to place the electrodes material in a neutral strain plane. Moreover, this bending test represents an extreme situation for these electrodes. For instance, during recordings from cortex surface, the curvature is smaller (larger bending radius) and the electrodes are fixed in one position.

We also measured the noise in saline solution for the different electrodes. Root-mean-square noise calculated from IZO, AgNWs11 +IZO, and AgNWs20 + IZO was 6.6± 2 µV, 8.4± 2 µV, and 5.7±2 µV, respectively. As demonstrated in a previous work, the difference in noise values, for electrodes with different impedance, is minor (Neto et al., 2018).

The presence of light-induced artifacts was quantified during electrical recordings in saline solution while applying optogenetic excitation light (470 nm). Results are shown in Figure 4a-c including artifacts measured from Au, IZO 200 nm, and AgNWS11 + IZO electrodes.

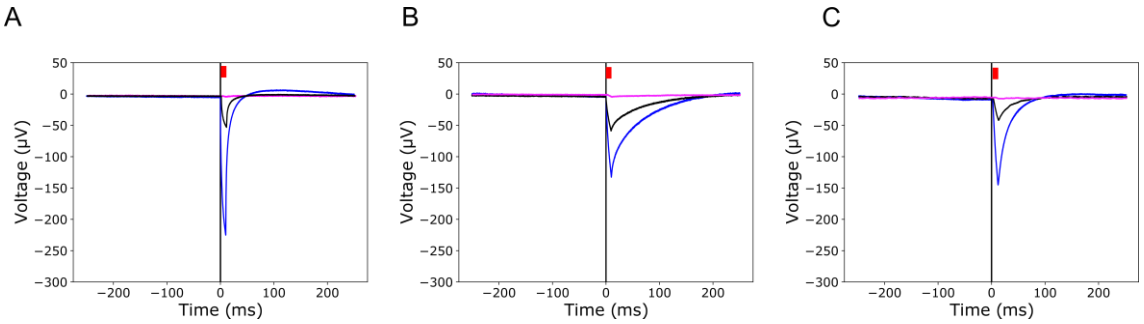

Figure 4. Light-induced artifact characterization. (a-c) Averaged light-induced artifact of Control Au, IZO 200 nm and AgNWS11+IZO representative electrode by varying light intensity. In each measurement a 10-ms light pulse was applied at 1 Hz for 1 min. The blue, black and magenta traces represent different light intensities. Blue: 95 mW/mm²; black: 23 mW/mm²; purple: 14 mW/mm². The red colored trace represents the light pulse (10 ms).

As expected, the artifacts increased with higher light intensity due to stronger photoelectric effects. For example, using 23 mW/mm^2 light, the artifacts (black lines in Figure 4) amplitude peak-to-peak measured from Au full-film microelectrodes was ~53 µV while those from IZO 200 nm and AgNWs11+IZO microelectrodes was about 63 and 38 µV, respectively. Our electrodes when compared with the metal grids electrodes (Qiang et al. 2018) have shown smaller artifacts for a given light intensity (using 20 mW/mm^2 the artifact amplitude was around 100 µV). We note that the amplitude of these artifacts for high light intensities are extremely sensitive to the relative position of the fiber tip (200 µm diameter) towards the electrode (500 µm diameter). Additionally, the peak-to-peak artifact amplitude using 14 mW/mm^2 is smaller than RMS noise (~5 µV) measured in saline solution.

Therefore, light-induced artifacts shouldn't be an issue for functional calcium imaging - widefield and 2-photon microscopy- where the illumination intensity is around 0.28 mW/mm^2 (Qiang et al., 2018). Moreover, for optogenetic stimulation of neurons where the power is higher, around 100 mW/mm^2, the light-evoked transient can be reduced by subtraction of the median of the activity across all channels (Jun et al., 2017).

In table 1, we summarized the transmittance, sheet resistance and impedance of IZO 200 nm and hybrid AgNWs + IZO electrodes to illustrate the trade-off between those parameters. We also benchmarked the performance of the fabricated electrodes against previous transparent electrodes. Our electrodes demonstrated comparable transmittance and impedance values, with improvements in the sheet resistance and CSC.

Table 1. Current transparent electrodes and their material, dimensions/area, impedance magnitude at 1 kHz in saline solution, sheet resistance and transmittance value at 550 nm. ⦰: diameter.

Work	Electrode Material	Dimensions Area	|Z| @ 1 kHz	Sheet resistance	Transmittance @ 550 nm
(Kuzum et al., 2014)	Doped Graphene	50 x 50 µm 2500 µm^2	~500 kΩ	Na	90 %
(P. Ledochowitsch, Olivero, Blanche, & Maharbiz, 2011) (P Ledochowitsch et al., 2015)	ITO	500 µm ⦰ 196350 µm^2	300 kΩ	43.7 Ω/sq	90 %

(Park et al., 2014)	Graphene	200 µm ⦸ 31416 µm²	243.5±5.9 kΩ	76 Ω/sq	~90%
(Thunemann et al., 2018)	Graphene	100 x 100 µm 10000 µm²	> 963 kΩ	Na	90 %
(Kunori & Takashima, 2015b)	ITO	250 µm ⦸ 49087 µm²	10-50 kΩ	200 Ω/sq	80 %
(Seo et al., 2017)	Au grid	80 x 80 µm 6400 µm²	127.19 kΩ	18 Ω/sq	70 %
(Qiang et al., 2017)	Au grid + PEDOT	80 x 80 µm 6400 µm²	11 kΩ	Na	70 %
(Lu et al., 2018)	Graphene 30 sec	100 x 100 µm 10000 µm²	15 kΩ	Na	50 %
Our work	IZO 100 nm	500 µm ⦸	452 kΩ	53 Ω/sq	82 %
	IZO 200 nm	500 µm ⦸	40.7 kΩ	25 Ω/sq	76 %
	AgNWs11 +IZO	500 µm ⦸	23 kΩ	23 Ω/sq	74 %
	AgNWS20+IZO	500 µm ⦸	20 kΩ	6 Ω/sq	62 %

Characterization of electrodes in vivo - electrical recordings

To demonstrate the in vivo performance of transparent electrodes fabricated with AgNWs 20 cycles + IZO films, we recorded electrical neural activity from a rat cortex surface.

Figure 5 A-B shows the surgery procedure, the position of electrodes and craniotomy. Figure 5B demonstrate the clarity of the electrodes and the ability to view the underlying cortex and cerebral vasculature through the prototype. Cortical electrical potentials recorded by AgNWs 20 cycles + IZO electrodes are shown in Figure 5 C. The electrical signal shows spontaneous cortical activity recorded under urethane anaesthesia without any sensory stimulus.

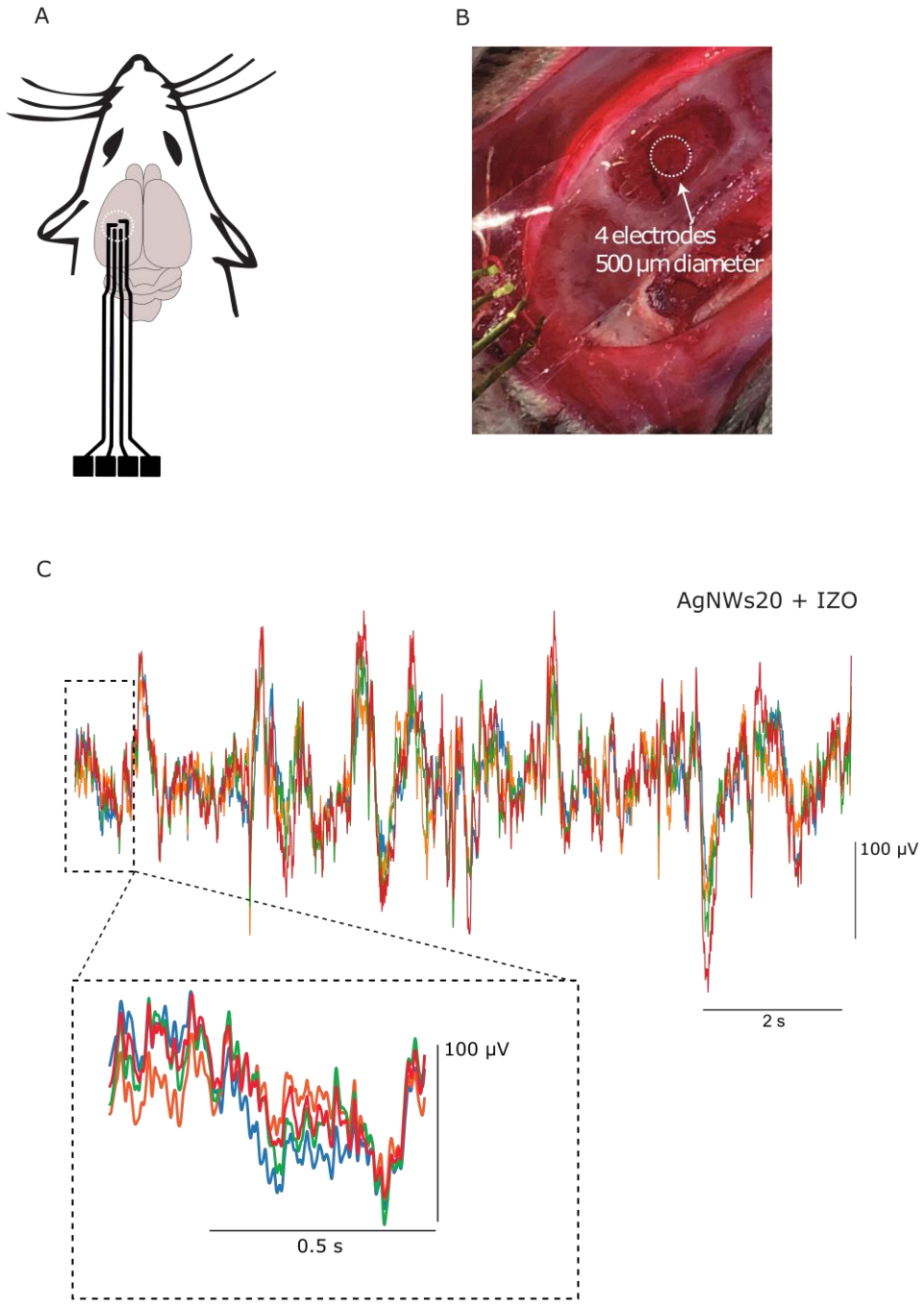

Figure 5. Characterization of electrodes in vivo. (a) Scheme of neural recordings, showing the surgery procedure; (b) Photograph of electrodes array on the cortex of rat above dura; (c) Low-passed (100 Hz) signal from hybrid AgNWs 20 cycles + IZO prototype.

Optical imaging characterization

Next, we enquired to which extent the presence of the films causes obstruction of light during fluorescence microscopy. Firstly, we coated cover slips with the films under study and then, we cover slipped brain slices expressing mCherry (excitation ~ 550 nm, emission ~ 600 nm) in neurons of the Lateral Posterior nucleus of the thalamus (LP) and several areas of the neocortex, and fluorescent dye (excitation ~ 358 nm, emission ~ 461 nm) in all neurons (Figure 6A). Confocal microscopy images (Figure 6B) suggest that AgNWs20 + IZO films have no impact on the imaging. Intensity profiles of neurons somas, across x and y axis, and along Z axis were plotted to quantify the full width at half-maximum (FWHM) obtained through hybrid films. The FWHM values for somas imaged trough glass (control) and hybrid films (AgNWs20 + IZO) were similar in all axes (0- to 1.6-fold difference).

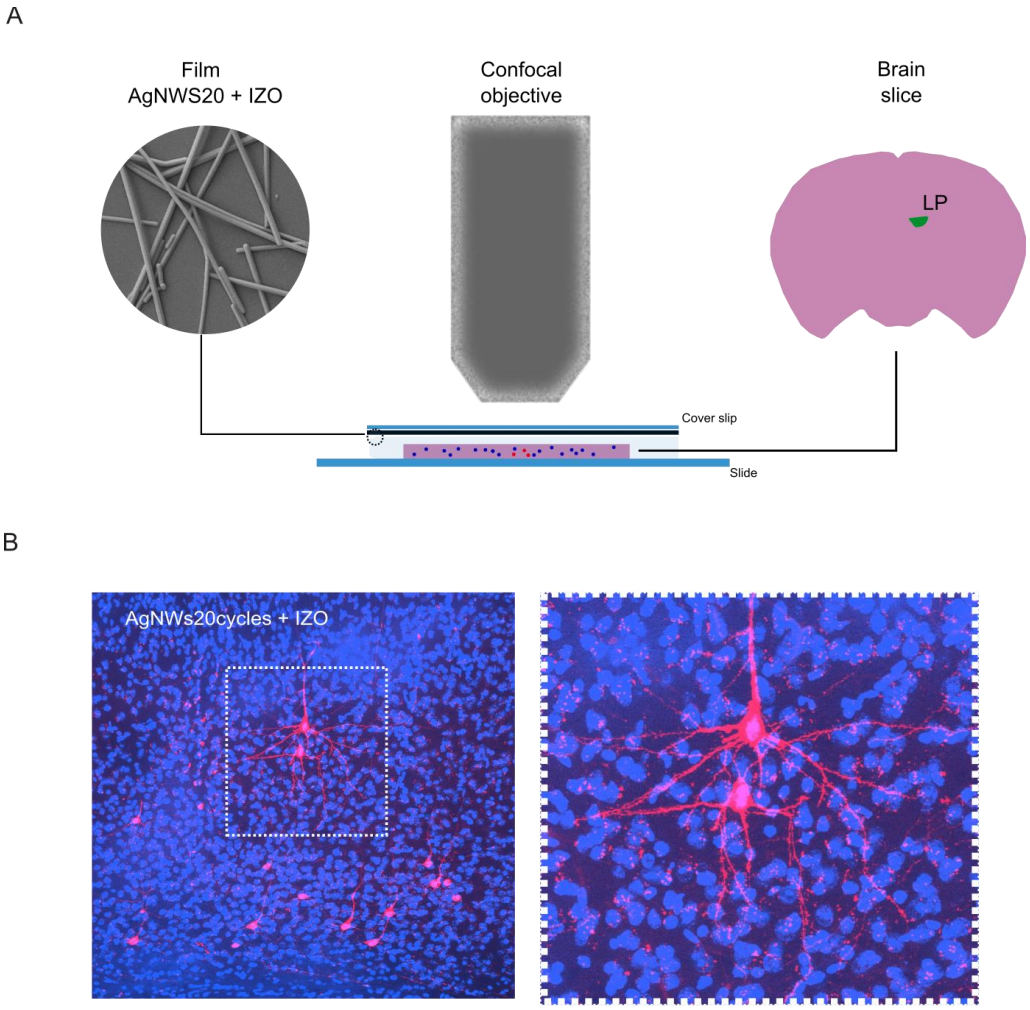

Figure 6. Optical imaging with confocal microscopy. (a) Schematic illustration of the confocal microscopy setup. A mouse brain slice was mounted on a glass slide and it was covered with a cover slip coated with the film under study. Note that excitation as well as emission light passes through films; (b) Multiples cells can be clearly imaged through the film.

Conclusions

We demonstrated a novel transparent and conductive material for ECoG microelectrodes with low impedance and high transmittance, which can be used for multimodal data acquisition (electrophysiology with optical imaging).

The hybrid microelectrodes formed by depositing IZO onto random networks of AgNWs demonstrated transparency over a broad optical window (200 to 1200 nm), with over 60% transmittance at 550 nm, which is slightly lower compared to the graphene or ITO microelectrodes but still sufficient for optical measurements. Nevertheless, the films produced with our hybrid material shown the lowest sheet resistance achieved in current transparent ECoG electrodes, as can be verified in Table 1.

Further studies will develop large-scale, high-density microelectrode arrays from this material for in vivo recordings with simultaneous optical imaging for increasing our understanding of the nature of the recorded signal and have an impact on clinical and brain-machine research where ECoG is frequently used.

Moreover, due to the ceramic nature of IZO and manufacturing costs, new materials and fabrication processes are being studied to replace this material in the hybrid films.

Acknowledges

We would like to thank the institutional support and funding provided by Sainsbury Wellcome Centre (funded by the Gatsby Charitable Foundation and the Wellcome Trust). This work was also funded by FEDER funds through the COMPETE 2020 Programme and National Funds through FCT - Portuguese Foundation for Science and Technology under the project number POCI-01-0145-FEDER-007688, Reference UID/CTM/50025. Moreover, this work received funding from the European Community's H2020 program under grant agreement No. 716510 (ERC-2016-STG TREND) and No. 685758 (1D-Neon).

We are very grateful to George Dimitriadis and Lorenza Calcaterra for animal experiment support. We also thank Tiago Mateus, Ana Santa, Inês Martins, Cátia Figueiredo, Tomás Calmeiro and Daniela Gomes for technical support.

References

Buzsáki, G. (2004). Large-scale recording of neuronal ensembles. *Nature Neuroscience*, *7*(5), 446–451. https://doi.org/10.1038/nn1233

Chung, T., Wang, J. Q., Wang, J., Cao, B., Li, Y., & Pang, S. W. (2015). Electrode modifications to lower electrode impedance and improve neural signal recording sensitivity. *Journal of Neural Engineering*, *12*(5), 056018. https://doi.org/10.1088/1741-2560/12/5/056018

Dimitriadis, G., Neto, J. P., Aarts, A., Alexandru, A., Ballini, M., Battaglia, F., … Kampff, A. R. (2018). Why not record from every channel with a CMOS scanning probe? *BioRxiv*, 275818. https://doi.org/10.1101/275818

Harris, K. D., Quiroga, R. Q., Freeman, J., & Smith, S. L. (2016). Improving data quality in neuronal population recordings. *Nature Neuroscience*, *19*(9), 1165–1174. https://doi.org/10.1038/nn.4365

Hecht, D. S., Hu, L., & Irvin, G. (2011, April 5). Emerging transparent electrodes based on thin films of carbon nanotubes, graphene, and metallic nanostructures. *Advanced Materials*.

John Wiley & Sons, Ltd. https://doi.org/10.1002/adma.201003188

Jun, J. J., Steinmetz, N. A., Siegle, J. H., Denman, D. J., Bauza, M., Barbarits, B., … Harris, T. D. (2017). Fully integrated silicon probes for high-density recording of neural activity. *Nature*, *551*(7679), 232–236. https://doi.org/10.1038/nature24636

Kozai, T. D. Y., & Vazquez, A. L. (2015). Photoelectric artefact from optogenetics and imaging on microelectrodes and bioelectronics: new challenges and opportunities. *Journal of Materials Chemistry B*, *3*(25), 4965–4978. https://doi.org/10.1039/c5tb00108k

Kunori, N., & Takashima, I. (2015a). A transparent epidural electrode array for use in conjunction with optical imaging. *Journal of Neuroscience Methods*, *251*, 130–137. https://doi.org/10.1016/J.JNEUMETH.2015.05.018

Kunori, N., & Takashima, I. (2015b). A transparent epidural electrode array for use in conjunction with optical imaging. *Journal of Neuroscience Methods*, *251*, 130–137. https://doi.org/10.1016/J.JNEUMETH.2015.05.018

Kuzum, D., Takano, H., Shim, E., Reed, J. C., Juul, H., Richardson, A. G., … Litt, B. (2014). Transparent and flexible low noise graphene electrodes for simultaneous electrophysiology and neuroimaging. *Nature Communications*, *5*(1), 5259. https://doi.org/10.1038/ncomms6259

Ledochowitsch, P., Olivero, E., Blanche, T., & Maharbiz, M. M. (2011). A transparent µECoG array for simultaneous recording and optogenetic stimulation. In *2011 Annual International Conference of the IEEE Engineering in Medicine and Biology Society* (pp. 2937–2940). IEEE. https://doi.org/10.1109/IEMBS.2011.6090808

Ledochowitsch, P, Yazdan-Shahmorad, A., Bouchard, K. E., Diaz-Botia, C., Hanson, T. L., He, J.-W., … Maharbiz, M. M. (2015). Strategies for optical control and simultaneous electrical readout of extended cortical circuits. *Journal of Neuroscience Methods*, *256*, 220–231. https://doi.org/10.1016/j.jneumeth.2015.07.028

Ledochowitsch, Peter, Olivero, E., Blanche, T., & Maharbiz, M. M. (2011). A transparent μECoG array for simultaneous recording and optogenetic stimulation. In *2011 Annual International Conference of the IEEE Engineering in Medicine and Biology Society* (pp. 2937–2940). IEEE. https://doi.org/10.1109/IEMBS.2011.6090808

Lee, H. J., Hwang, J. H., Choi, K. B., Jung, S.-G., Kim, K. N., Shim, Y. S., … Ju, B.-K. (2013). Effective Indium-Doped Zinc Oxide Buffer Layer on Silver Nanowires for Electrically Highly Stable, Flexible, Transparent, and Conductive Composite Electrodes. *ACS Applied Materials & Interfaces*, *5*(21), 10397–10403. https://doi.org/10.1021/am4025802

Lima, S. Q., Hromádka, T., Znamenskiy, P., & Zador, A. M. (2009). PINP: A New Method of Tagging Neuronal Populations for Identification during In Vivo Electrophysiological Recording. *PLoS ONE*, *4*(7), e6099. https://doi.org/10.1371/journal.pone.0006099

Lopes, G., Bonacchi, N., Frazão, J., Neto, J. P., Atallah, B. V., Soares, S., … Kampff, A. R. (2015). Bonsai: An event-based framework for processing and controlling data streams. *Frontiers in Neuroinformatics*, *9*(APR). https://doi.org/10.3389/fninf.2015.00007

Lu, Y., Liu, X., Hattori, R., Ren, C., Zhang, X., Komiyama, T., & Kuzum, D. (2018). Ultralow Impedance Graphene Microelectrodes with High Optical Transparency for Simultaneous Deep Two-Photon Imaging in Transgenic Mice. *Advanced Functional Materials*, *28*(31), 1800002. https://doi.org/10.1002/adfm.201800002

Neto, J. P., Baião, P., Lopes, G., Frazão, J., Nogueira, J., Fortunato, E., … Kampff, A. R. (2018). Does Impedance Matter When Recording Spikes With Polytrodes? *Frontiers in Neuroscience*, *12*, 715. https://doi.org/10.3389/fnins.2018.00715

Neto, J. P., Lopes, G., Frazão, J., Nogueira, J., Lacerda, P., Baião, P., … Kampff, A. R. (2016). Validating silicon polytrodes with paired juxtacellular recordings: method and dataset. *Journal of Neurophysiology*, *116*(2), 892–903. https://doi.org/10.1152/jn.00103.2016

Park, D.-W., Schendel, A. A., Mikael, S., Brodnick, S. K., Richner, T. J., Ness, J. P., … Williams, J. C. (2014). Graphene-based carbon-layered electrode array technology for neural imaging and optogenetic applications. *Nature Communications*, *5*(1), 5258.

https://doi.org/10.1038/ncomms6258

Qiang, Y., Artoni, P., Seo, K. J., Culaclii, S., Hogan, V., Zhao, X., … Fang, H. (2018). Transparent arrays of bilayer-nanomesh microelectrodes for simultaneous electrophysiology and two-photon imaging in the brain. *Science Advances*, *4*(9), eaat0626. https://doi.org/10.1126/sciadv.aat0626

Qiang, Y., Seo, K. J., Zhao, X., Artoni, P., Golshan, N. H., Culaclii, S., … Fang, H. (2017). Bilayer Nanomesh Structures for Transparent Recording and Stimulating Microelectrodes. *Advanced Functional Materials*, *27*(48), 1704117. https://doi.org/10.1002/adfm.201704117

Sanders, J. I., & Kepecs, A. (2014). A low-cost programmable pulse generator for physiology and behavior. *Frontiers in Neuroengineering*, *7*, 43. https://doi.org/10.3389/fneng.2014.00043

Scanziani, M., & Häusser, M. (2009). Electrophysiology in the age of light. *Nature*, *461*(7266), 930–939. https://doi.org/10.1038/nature08540

Seo, K. J., Qiang, Y., Bilgin, I., Kar, S., Vinegoni, C., Weissleder, R., & Fang, H. (2017). Transparent Electrophysiology Microelectrodes and Interconnects from Metal Nanomesh. *ACS Nano*, *11*(4), 4365–4372. https://doi.org/10.1021/acsnano.7b01995

Thunemann, M., Lu, Y., Liu, X., Kılıç, K., Desjardins, M., Vandenberghe, M., … Kuzum, D. (2018). Deep 2-photon imaging and artifact-free optogenetics through transparent graphene microelectrode arrays. *Nature Communications*, *9*(1), 2035. https://doi.org/10.1038/s41467-018-04457-5

Yun, H. J., Kim, S. J., Hwang, J. H., Shim, Y. S., Jung, S. G., Park, Y. W., & Ju, B. K. (2016). Silver nanowire-IZO-conducting polymer hybrids for flexible and transparent conductive electrodes for organic light-emitting diodes. *Scientific Reports*, *6*. https://doi.org/10.1038/srep34150

Yuste, R. (2015). From the neuron doctrine to neural networks. *Nature Reviews Neuroscience*, *16*(8), 487–497. https://doi.org/10.1038/nrn3962

Supplementary Information

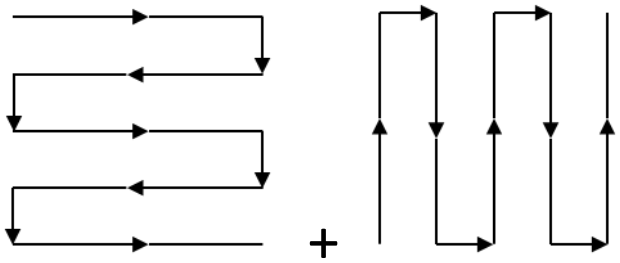

Figure 1. Scheme of one cycle of AgNWs spray deposition.

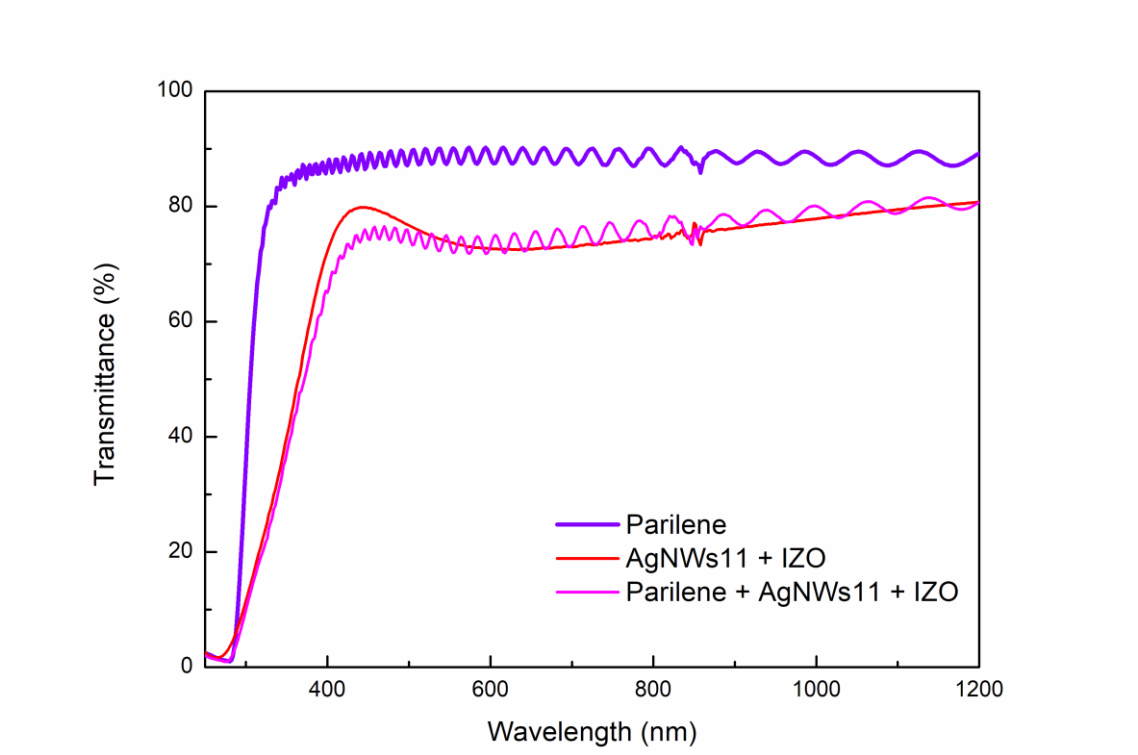

Figure 2. Optical transmittance of hybrid films (AgNWs with IZO) on parylene.

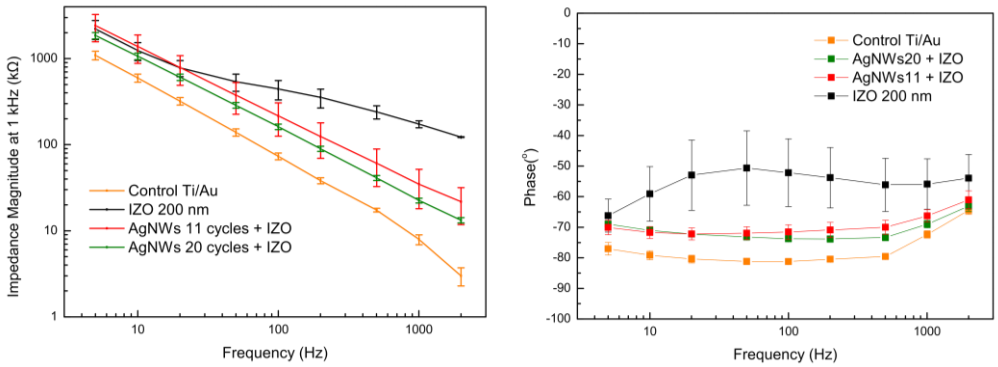

Figure 3. Electrochemical impedance spectroscopy (EIS) of prototypes with IZO 200 nm, hybrid (AgNWs with IZO) and Au electrodes, respectively.

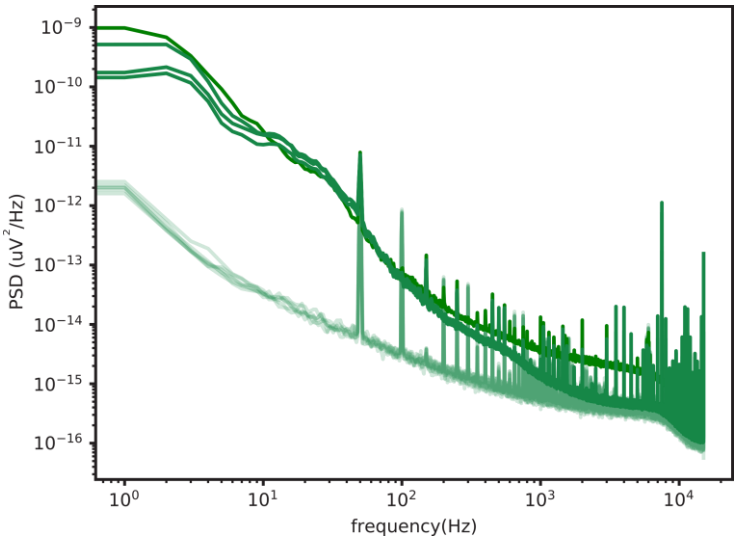

Figure 4. Signal power spectra density (PSD) for AgNWs 20 cycles + IZO electrodes in saline and in vivo under urethane. The difference in signal power at lower-frequency band, in saline and in vivo, is significantly in the low frequency range.

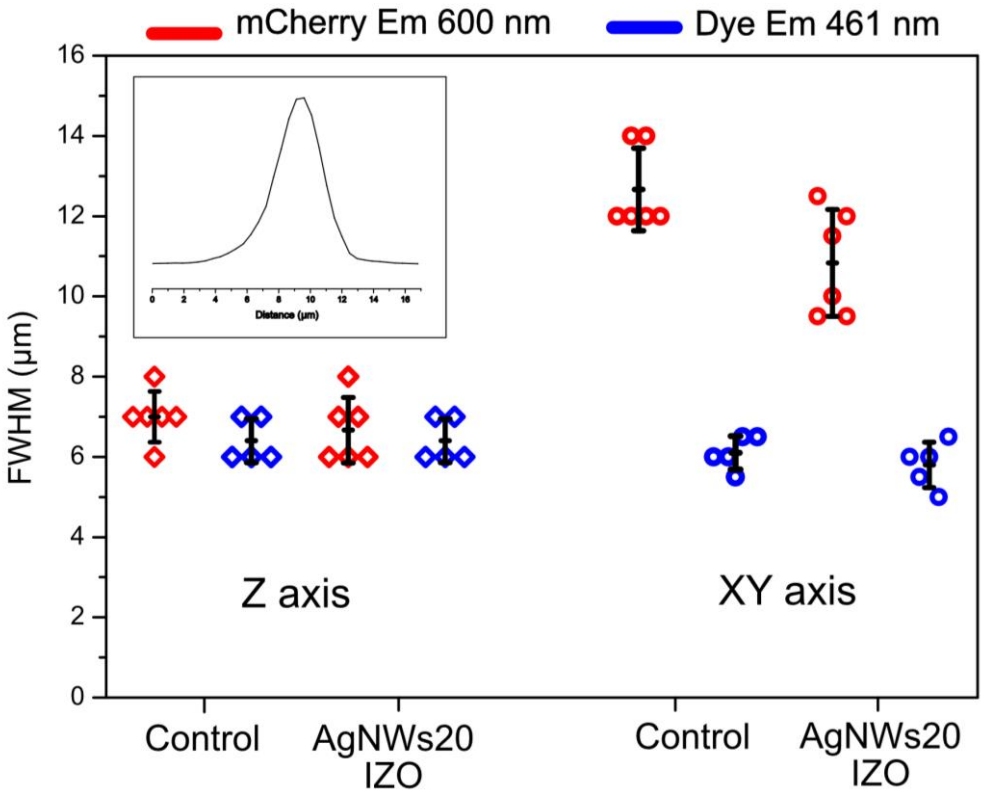

Figure 5. Quantification of full width at half-maximum (FWHM) of neurons expressing mCherry (red) and dye (blue) imaged trough glass (control) and hybrid films (AgNWs20 + IZO). The intensity profiles of neurons somas were plotted across x and y axis and along Z axis using Image J (plot XY profile and plot Z-axis profile within a rectangular selection surrounding soma). Inset shows a representative intensity profile in Z axis from a neuron expressing mCherry. Mean ± standard deviation per condition are shown.